

Douglas Chinn*
e-mail: dachinn@sandia.gov
Sandia National Laboratories,
P.O. Box 5800, MS0603 Albuquerque,
NM 87185

Peter Ostendorp
Dartmouth College,
HB 8000, Hanover,
NH 03755

Mike Haugh
Russell Kershmann

Resolution Sciences Corporation,
685 Northern Ave., Mill Valley,
CA 94941

Thomas Kurfess

Andre Claudet

Thomas Tucker

Georgia Institute of Technology,
Woodruff School of Mechanical Engineering,
Atlanta, GA 30332

Three Dimensional Imaging of LIGA-Made Microcomponents

Nickel and nickel-alloy microparts sized on the order of 5–1000 microns have been imaged in three dimensions using a new microscopic technique, Digital Volumetric Imaging (DVI). The gears were fabricated using Sandia National Laboratories' LIGA technology (lithography, molding, and electroplating). The images were taken on a microscope built by Resolution Sciences Corporation by slicing the gear into one-micron thin slices, photographing each slice, and then reconstructing the image with software. The images were matched to the original CAD (computer aided design) model, allowing LIGA designers, for the first time, to see visually how much deviation from the design is induced by the manufacturing process. Calibration was done by imaging brass ball bearings and matching them to the CAD model of a sphere. A major advantage of DVI over scanning techniques is that internal defects can be imaged to very high resolution. In order to perform the metrology operations on the microcomponents, high-speed and high-precision algorithms are developed for coordinate metrology. The algorithms are based on a least-squares approach to data registration the $\{X, Y, Z\}$ point clouds generated from the component surface onto a target geometry defined in a CAD model. Both primitive geometric element analyses as well as an overall comparison of the part geometry are discussed. Initial results of the micromasurements are presented in the paper.

[DOI: 10.1115/1.1812774]

Introduction

Large-scale machines such as turbine blades, gears, precision ball bearing surfaces, injection molds, and automotive bodies can be measured with relative ease and high accuracy using today's technologies. A variety of metrology systems have been developed to take coordinate information directly from the surface of a manufactured part such as a coordinate measurement machine (CMM) or a laser scanner. Nominally, these systems are employed in parts having a size scale of 10 mm or larger. However, for small-scale geometries (i.e., microelectromechanical systems (MEMS)) such a technology does not exist.

Accordingly, a nondimensional comparison makes current tolerances of MEMS products comparable to tolerances achievable in 18th century. The small size of MEMS products either makes them inaccessible for existing metrology instruments or makes the use of such instruments inefficient. Micromachines are rapidly moving from the laboratory to the marketplace, consequently the need for precise metrology has come about. However, the success of micromachines has been severely limited by the fact that there presently exists no means to inspect microcomponents consisting of complex geometries. This eliminates the possibility of feedback based on geometry for component quality control. The lack of such a capability results in two major issues for microfabrication. First, there is no means to verify that a part is produced correctly, resulting in decreased yield rates. Second, only simple parts such as prismatic components that are 2 or 2.5 dimensions (2D) in nature can be produced with high confidence and high yield rates using tools adapted from the semiconductor industry.

A typical integrated circuit (IC) these days has linewidths in the

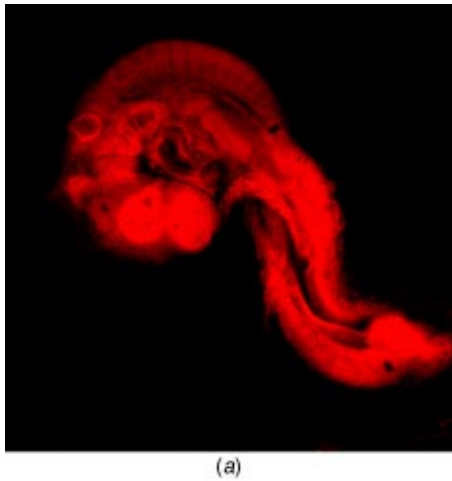
x - y plane below 1 micron, and film thicknesses perpendicular to the wafer plane on the order of 0.1–1.0 micron. IC's are 2D *microscale* objects, scaled from 0.1 to 100 microns. Many manufacturers offer machinery for measuring on these scales with a high level of accuracy and repeatability.

With three dimensional (3D) *mesoscale* (1 micron to 10 mm in x , y , and z dimensions) parts and devices, new techniques are needed to measure and evaluate the manufacturing process. Advances in feature-based metrology and computational geometry have changed the paradigm for the inspection of large-scale complex geometries. Where feature precision is concerned, a single scalar measurement is no longer enough information to adequately describe a complex geometry. Two-dimensional devices can be understood with one-dimensional measurements. Three-dimensional parts require 2D information, or a picture, to describe them. A gear, for instance, requires multiple measurements, including hub diameter, pitch, addendum and dedendum circles, involutes, top and bottom surface finish, sidewall finish, sidewall angle and tooth thickness, radius of curvature, and circularity. In addition, for reliability, information about the *internal* structure of the part is of great importance. All manufacturing processes have bias and error, and although topside measurements are taken throughout the process, no information is obtainable about the deep holes and sidewalls until finished parts are available after release from the substrate.

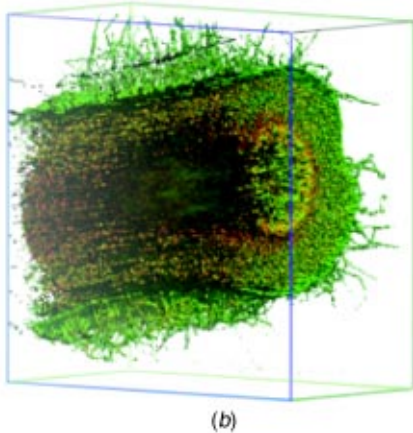
The challenges of imaging complex shapes with dimensions below 10 mm are considerable. First, handling and holding the sample can be problematic. Any technique to mechanically grip the part will distort it, and hide part of the device from the light source. Vacuum techniques do not work on trusslike parts, and adhesives can distort parts and leave residues. Other problems related to imaging small parts involve moving them so that each side can be imaged and getting images from the inside of holes

*Corresponding author.

Contributed by the Manufacturing Engineering Division for publication in the JOURNAL OF MANUFACTURING SCIENCE AND ENGINEERING. Manuscript received February 9, 2004; revised September 1, 2004. Associate Editor: J. Ni.



(a)



(b)

Fig. 1 (a) 3D images of tissues. A false color chick embryo. (b) A plant root, also in false color. The “bounding box” surrounding the object is an aid to the eye and can be removed with software. Further processing can enhance different details of objects imaged with DVI.

[1]. If the part is simply set on a stage, it cannot be manipulated to see the sides and bottom. Moving the imaging lens presents a new set of problems.

Examining these parts with any microscope using a point source of illumination gives a 2D picture, and determining the exact location of a rounded edge is difficult. Plus, depth-of-field limitations prevent a complete picture from emerging. Scanning electron microscope (SEM) studies are useful, but still give a distorted 2D image that cannot be rotated or examined. Any technique that uses a point source of photons for the stimulus cannot have information return to the imaging optics from surfaces more than about 10 deg away from vertical. No information about the interior of the part is available with low-energy photons.

Three-dimensional imaging is well developed by the medical industry [2]. To obtain useful information, 3D imaging operations have been divided into four categories [3]: preprocessing, visualization, manipulation, and analysis. There are a number of evolving techniques that can digitize the surface of a microcomponent, generating thousands or even millions of $\{X,Y,Z\}$ data points from the surface of a part which are currently being studied to do these operations on micromachines, among them holography [4] and x-ray techniques [5] and a CMM using a silicon cantilever microprobe work [6].

Ideally, micron resolution over a scale of 1000 microns in all three coordinate axes is desirable. The only technique available today is Digital Volumetric Imaging (DVI), which was originally developed for imaging tissue samples [7]. There has been particu-

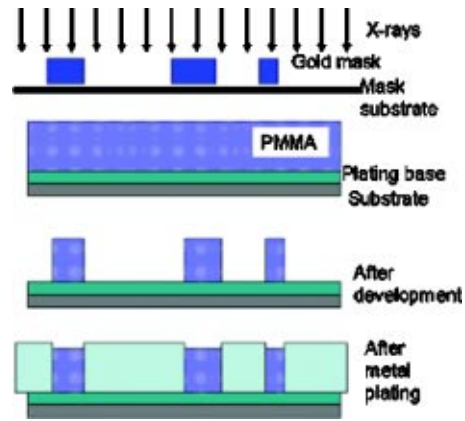


Fig. 2 The LIGA process. After plating, the PMMA is dissolved and the parts are released from the substrate.

lar success for the 3D imaging of developing embryos [8]. Figure 1(a) is an example of a chick embryo where the eye and spine can clearly be seen, and Fig. 1(b) is an example of a plant stem. Considerably more detail is available than can be seen in these images. Inorganic materials as diverse as paper and a cotton swab have also been imaged. DVI solves the problems listed above by embedding the part in a matrix. At the scales we are interested in the matrix will not distort the metal object sufficiently to matter, and moving the part is unnecessary since the whole device is imaged and can be viewed at all angles and internally with the software. Besides being able to measure parts in 3D within RES-View (the DVI software), a point cloud of the surface can be extracted and compared to a model. DVI is a destructive technique, but it allows for the 3D rendering of internal defects at very high resolution. The loss of a single sample in a mass produced part is a small trade-off for the unique information available. Destructive metrology is common in medicine; for example, biopsy analysis by histologic microscopy is destructive to both the patient and the sample, but remains the standard of diagnosis in much of modern medicine. SEM analysis can also be considered destructive, since metal plating and mounting of parts can render them useless for their intended purpose.

In this paper we discuss a new technique to image hard metal micromachines fabricated using the LIGA process at Sandia National Laboratories in California. Sample preparation and imaging take about a day, similar to transmission electron microscope (TEM) analysis. Measurement errors are determined by calibrating the system with ball bearings, the most precise 3D objects we have been able to identify.

The LIGA Process

LIGA is a micromachining technique that does not fit well into either of the two principle methods of miniature manufacturing, surface and bulk micromachining [9]. Figure 2 shows a cross-section of the LIGA manufacturing process. A metal plating base is deposited on a substrate, typically silicon. A PMMA (poly methyl methacrylate or Plexiglas) sheet is glued onto the substrate. After being machined to the correct thickness, the wafer is exposed to a high-energy (10-keV) x-ray beam generated in a synchrotron. The mask used to block the x-rays and define the pattern is a gold film on a thin (low-Z) silicon substrate. The advantage of LIGA over UV lithography is the ability to expose very thick resists and the ability to achieve very vertical sidewalls in the completed parts.

After exposure, the pattern is developed in an organic solution, leaving a deep PMMA mold on a metal plating base. The mold is filled in with metal by electroplating. Nickel is the most common metal but other metals, such as copper, nickel-iron, or nickel cobalt are sometimes used. Due to nonuniform current density in the

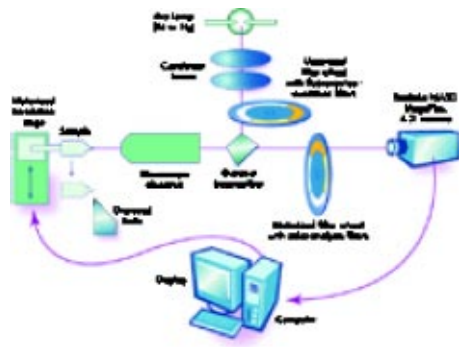


Fig. 3 A schematic of the Digital Volumetric Imaging process

plating bath, the mold is overplated, requiring a final lapping to make the surface uniform. The individual piece parts are released from the substrate, sorted, and shipped to the customer. Sandia has achieved molds over 1000 μm deep, although typical parts are 300–800 μm thick, with dimensions in the plane of the wafer varying from a few microns to millimeters. Linewidth is determined by the resolution achievable on the gold mask. The mask is made using conventional UV (365-nm) lithography in thick, positive photoresists. A gold thickness of $\sim 20 \mu\text{m}$ is typically used, limiting horizontal resolution to ~ 5 microns. The best aspect ratio achieved is better than 10:1 [10].

DVI 3D Metrology Experimental Setup

The DVI Process and Apparatus. The Digital Volumetric Imaging process that was used to image LIGA parts is an application of Block Face Imaging, a patented technology [11] for generating a stack of 2D digital images that are properly registered and can be converted into a fully three-dimensional digital data set. The 2D images are obtained using a light microscope. The sample that is to be imaged is first embedded in an appropriate solid medium referred to as the sample block. The sample block is mounted in the optical apparatus and the face of the block is prepared by removing the excess front surface. The block face is illuminated and a 2D image is taken of the freshly cut face, either in fluorescence or reflection mode or both. Monochromatic or multicolor images can be generated. The slices removed can be saved for chemical analysis, if desired. The proprietary embedding medium is designed so that the fluorescence or reflection comes only from the front surface of the sample. After the images are taken, a microtome cuts a controlled thickness from the front surface (sectioning). A second 2D image is taken. This process of surface removal and imaging is continued until the embedded sample is completely imaged. The system is illustrated in Fig. 3. The stack of 2D images is then converted into a 3D data set. This data set can then be viewed as a 3D object from any orientation and 2D cross sections can be viewed at any location within the object [12]. Measurements can be made on these images and various analyses can be performed.

The Resolution Sciences Corp. Digital Volumetric Imaging system comprises an optical microscope, a microtome for block face cutting, a robotic motion control system, a digital camera, a frame grabber, and a personal computer that provides image collection, supervisory control and user interface (Fig. 3).

The optical system is a modified Nikon fluorescence microscope. The illumination source can be either a xenon or mercury arc lamp. Filters are used to select the desired illumination wavelength bands. A wavelength-selective beam splitter reflects the illumination beam into a standard microscope objective lens that focuses the beam onto the block face. The fluorescent or reflected light coming from the block face returns through the objective lens and is converted into an approximate plane wave. The beam splitter transmits this beam to a rotating filter wheel that selects

Table 1 Magnification, field of view and resolution of images

Objective lens magnification	FOV (mm)	Resolution ($\mu\text{m}/\text{pixel}$)
2 \times	8.8	4.4
4 \times	4.4	2.2
10 \times	1.77	0.88
20 \times	0.88	0.44
40 \times	0.44	0.22

the desired wavelength bands to produce multicolored images. A set of lenses focuses the beam onto the CCD chip of the Kodak 2029 \times 2044 pixel digital camera, model Megaplus 4.21.

The block face is sectioned with a diamond knife using a robotically controlled microtome (Olympus, Melville, NY). The microtome moves the sample toward the cutting plane a distance equivalent to the cut thickness. It then moves the sample across the knife edge to cut sections from the block surface that range from 0.25 to 4.4 μm in thickness. The microtome then returns the block face to the imaging position with reproducibility better than 100 nm.

Supervisory control is done through a personal computer. The robotic control uses a DCX-AT2000 motion control board from Precision MicroControl (Carlsbad, CA) that is located in the PC. It controls a filter wheel, a shutter, and the vertical and forward movements of the sample block by the microtome. Stepper motors are used. The PC also houses a PCI_DVK digital camera interface board from Engineering Design Team (Beaverton, OR). The PC does the image collection and provides a user interface.

Sectioning the Block Face. Cutting the LIGA parts and other hard materials for DVI imaging presents challenges. The microtome technology was developed for cutting biological materials. TEM users in the materials science have begun to apply this technology in the past two decades [13–16] to some very hard materials with success as new techniques were developed. Although their cut sizes needed for TEM are much smaller, 0.1 μm square by 30 nm thick, and therefore they use an ultramicrotome, we have been guided by their experience. DVI images samples have millimeter dimensions and minimum cut thicknesses of 200 nm with thousands of cuts for each 3D image. The sample is first embedded in a plastic block that can be mounted in the microtome chuck. The several types of cutting problems that had to be solved include knocking the remaining section of the part out of the embedding material, knife nicks that produce striations on the block face alter the reflection characteristics of both the embedding medium and the sample, and a stick-slip cutting mechanism that produces a “washboard”-like surface on the embedding medium, altering its reflection characteristics. The latter two effects would damage image quality and prevent accurate determination of the sample surface. The stick-slip problem could be severe enough to bend the block and cause the knife to dig into the sample, stopping the microtome movement and damaging the sample. The proper choices of embedding material, surface adhesion additives, sample orientation, location of the sample in the block, and embedding technique are critical to successfully cutting these samples so that we obtain an accurate image. Development of reliable cutting methods has allowed us to cut and image many kinds of LIGA parts (copper and various nickel alloys) on a routine basis. Work remains to be done and will be the subject of a future paper.

Image Collection. A microscope objective lens is selected that will give the desired resolution and field of view (FOV). A compromise is generally required since higher resolution means a smaller field of view. Table I provides typical values. The image resolution is limited by the camera pixel resolution, given in col-

umn 3. The lens resolving power is greater than the pixel resolution for these lenses, although they are close at the $40\times$ resolution.

The sample block is mounted in the microtome and the motion control system moves it near the focal plane of the lens. The PC monitor shows a black and white image for each color so that the operator can focus the sample, adjust the camera gain and exposure, and monitor the system operation. A grid is embedded at the front of the block so that these gain and exposure adjustments are completed before the sample comes into view. The only image processing done at this stage is to replace bad camera pixels (pixels that have an excessive dark current drift). Upon completion of the imaging for the entire sample, the dataset, a stack of 2D images, is transferred over the network to another computer for image processing.

Image Processing. After the dataset is captured on the imaging machine, it is transferred to another PC dedicated to image processing. A variety of image processing tools are available, depending on the sample needs. The hard materials are usually cut at a thickness different from the pixel resolution so the appropriate number of frames can be averaged to produce a square voxel. Pixel drift can be corrected. Infrequently a residue from the cutting process sticks to the block face and shows in the image. This defect can be removed with the software, as can other noise. Defects can easily be seen with the eye as one “flies” through the image, making them easy to find and remove, or simply ignore (a few such defects in a thousand images does not affect the overall image). Registration shifts that occur if the imaging process is interrupted can be corrected. Many other tools are available, if needed. After the necessary image processing is completed, the final step converts the 2D stack into a proprietary 3D format. The sample can now be viewed as a full 3D image using the Resolution Sciences Corp. proprietary visualization software, RESView.

RESView: Viewing and Analyzing the 3D Image. The RESView software package allows the user to view the 3D image from many perspectives and to view 2D images cut through the object at any location within the object. The microscope system is calibrated so that accurate dimensional measurements can be made on the sample. Various tools for image analysis are available. For example, when multicolor images are analyzed, items can be segmented based on color, then counted and/or sized.

Two modes of imaging were tested for LIGA materials: a reflection mode where the sample had a high gray level and the background was dim, and a fluorescence mode where the embedding material was made fluorescent and had a high gray level and the sample was dark. The fluorescence mode was found best for samples having narrow regions and for frangible materials like silicon. The reflection mode is better for solid metal objects that do not have narrow regions and necessary if you want to observe internal cavity defects. The reflection mode was used for all the samples described in this paper.

The reflection images are monochromatic with the sample having a much higher gray level than the surrounding background. RESView allows you to separate the object from the background using a gray level threshold; all pixels above the threshold setting are retained and the remaining pixels are set to zero. Figure 4 shows a 3D image and 2D cross section a of a microgear, the former obtained using the threshold method. Segmenting the image, that is, isolating the sample from the background, has been developed considerably for 2D imaging [2]. The more sophisticated methods provide smoothing at the edge region to minimize noise, then use a derivative algorithm to locate the edge, often to a subpixel accuracy. To apply this approach to any image, a necessary requirement is that the image does not go into saturation in the region of the edge. For the LIGA parts in this cutting/imaging development stage, it was necessary to keep the image saturated. Also, 3D extensions of the 2D algorithms cited above have not yet been incorporated into RESView. For these reasons, segmentation

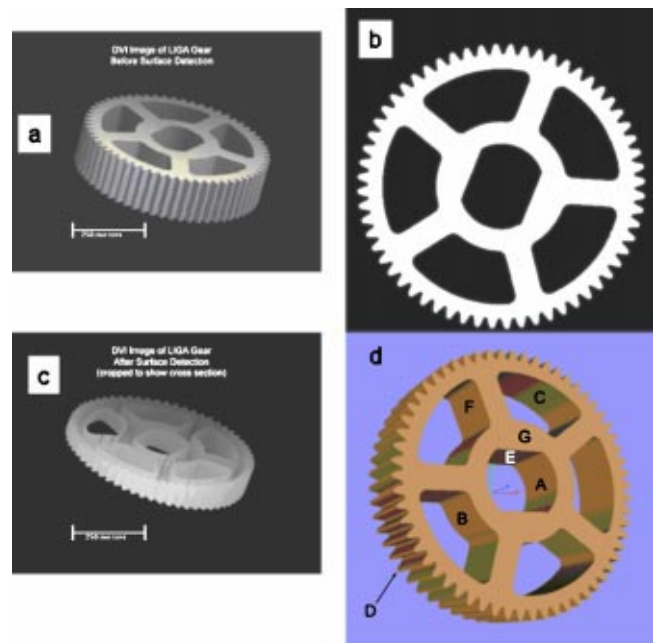


Fig. 4 (a) 3D image of LIGA gear: After the stack of 2D images has been converted to the proprietary format, a 3D image emerges. This 3D rendering can be cropped and rotated. (b) 2D cross section showing one slice of a gear. (c) Surface detection: RESView software performs an edge threshold surface detection algorithm on a 3D dataset, enabling the metrological inspection of complex 3D geometries. The above image of a LIGA gear has been cropped from above to demonstrate that interior image information has been removed, leaving only sidewalls. The surface generated is 1 voxel thick throughout. (d) CAD model of a gear. See Table 2 for details.

was done using an extension of the thresholding algorithm as described in the following paragraph. The edge detection accuracy for these images is on the order of ± 2 pixel for each edge. Future efforts to improve the image/cutting and the 3D edge detection will allow subpixel edge detection and dimensional accuracies of $1 \mu\text{m}$ or less.

A continuity requirement that all pixels above the threshold be continuous from the starting point (selected by the user) allows use of a lower threshold. This method was used to segment all solid samples for this paper. For example, a threshold value of 150 gray levels (8 bits) was used for the gear. Once the solid part has been segmented, surfaces can be isolated using a 3D form of a threshold edge detection algorithm in RESView. After reviewing a number of 2D images, the user sets a threshold at which the surface of the part is thought to exist. A binary mask of the 3D image is created. Voxels (3D pixels) whose intensity values are greater than or equal to the threshold are assigned a 1; voxels whose intensity values are less than the threshold are assigned a 0. The edge is defined as any “1-valued” voxel that has at least one face in contact with a “0-valued” voxel. The 3D image is then rendered displaying only the surfaces of the part. This is illustrated in Fig. 4(c).

Now that the critical surface detection step has been performed, RESView can export the 3D image in ASCII format as a cloud of Cartesian coordinates (point cloud). The 3D point cloud is imported into PARAFORM software and scaled according to the resolution at which it was imaged.

Discussion

Figure 4 shows data that were taken from a nickel-alloy microgear produced using the LIGA process. The point cloud shown in

consists of approximately 650,000 points, making it a relatively small point cloud. The major diameter of the gear is approximately 520 μm .

The gear was embedded in Resolution Science's epoxy polymer material and was mounted in the microtome holder. A 0.55-micron-thick section was cut from the top of the specimen using a 45-deg, atomically sharp diamond microtome blade. Approximately 500 images were taken using this method. The accumulated errors in the Z motion are a potential problem, but can be corrected for with the use of standard, accurate spheres. DVI is still a developmental technique, applying a life science imaging technique to hard materials. Future papers will be forthcoming.

Because the slice thickness of 0.55 μm differs from the CCD image resolution of 1.77 $\mu\text{m}/\text{pixel}$, it becomes necessary to average serial sections together to preserve isotropy of the entire 3D dataset, generating cubic voxels rather than rectangular prisms. Averaging intensity values between two or three thin sections is permissible because the vast majority of pixel intensity values among the serial sections are in the 254–255 range (these values occur along the interior of the cross section in areas of high reflectance).

The 3D gear image was then visually inspected using Resolution Science's RESView software, Fig. 4(a). With the exception of a few particles suspended inside the hub of the gear, the dataset was free of unwanted artifacts. The unwanted particles probably resulted from a polymer chip that clung to the block face after one of the sections was imaged. They were removed from the data using RESView's object isolation algorithm thresholded at full color range (0–256) in order to preserve edge information. The gear was thus isolated from any noise in the dataset. No surface artifacts resulting from the microtoming process could be detected.

In order to perform 3D metrology on the gear, part surfaces had to be isolated. RESView's edge threshold algorithm was used to determine the outer surfaces of the part. Figure 4(b) shows a cross section of the gear. To determine the appropriate threshold value for the algorithm, the edges of various cross section images were inspected to determine the range color values in the edge. These values ranged from approximately 150 along the outside surfaces to 254 on the part interior. A mean threshold value of 203 was chosen for the edge detection algorithm, yielding a 1-voxel-thick surface point cloud as shown in Fig. 4(c). To confirm that a valid edge threshold was chosen, the dataset was exported at various thresholds ranging from 0 to 254 (the highest color value in the dataset). Using different threshold values did not alter the measurements taken in Paraform (described below) beyond the volumetric resolution of 1.77 μm as long as the threshold was set using a value contained in the edge.

The voxel coordinate information was exported in an ASCII, point cloud format and was imported into Paraform's inspection module. The point cloud was scaled by a factor of 1.77 in order to allow for point-to-point calculations in units of microns. The original CAD model for the gold x-ray lithography mask (Fig. 4(d)) was then imported into Paraform for comparison. The extrusion height (height in the z direction along the axis of the gear) of this model was based on the intended, final lapped height of the finished gear, 150 μm .

After point cloud registration to the CAD model, Fig. 5, colored error maps were generated to show any normal point-to-surface deviations between the CAD model and the 3D data. Calculations were also performed to measure the dimensions of certain key geometries in the gear such as the hub radius, tooth thickness, addendum circle, and various sidewall angle deviations.

Analysis of Data

To validate component geometry in three-dimensional space, the point cloud that is generated (e.g., $\{X, Y, Z\}$ points from the surface of the part) must be compared to a CAD model. Two major issues must be addressed for this comparison. The first is to

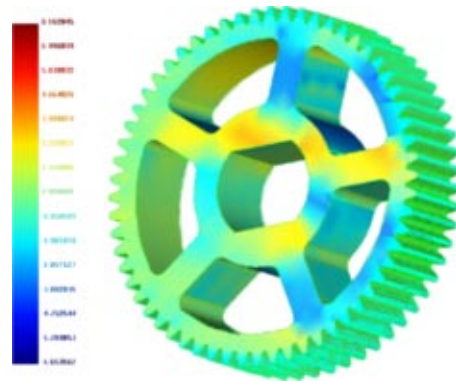


Fig. 5 Error map: By performing normal point-to-surface calculations, Paraform's inspection module creates an error map of the LIGA gear that shows clearly where deviations from design geometry occur. Deviations are strongest near the gear hub. The error scale is in units of microns.

align the point cloud and the CAD model into the same reference frame. This process is called registration and is equivalent to fixturing or datuming when inspecting on a CMM. The second issue is the assignment of each point to the proper surface of the CAD model. This paper addresses registration. For a treatment of the point to surface assignment see Refs. [17,18].

The mathematical basis for point cloud to CAD model registration is based on a least squares optimal fit minimizing the normal distance between each point to the closest surface of the model. Consider a set of n coordinate data points, $P = \{p_1, p_2, \dots, p_n; p_i \in \mathcal{R}^3\}$, measured from a surface, S , modeled by the parametric equation $S(u, v)$ that maps the parameters $u \in \mathcal{R}$ and $v \in \mathcal{R}$ in \mathcal{R}^3 . The distance from a given point p_i in P to S is defined as the magnitude of the vector from the closest point on S to p_i and is depicted by the magnitude of d_i in Eq. (1).

$$\|d_i\| = \min_{u, v} \|p_i - S(u, v)\| \quad (1)$$

The u and v that provide the solution to the minimization in Eq. (1) clearly depend on the value of p_i , and therefore, the optimal u and v are a function of p_i . These optimal values are hereafter referred to as u_{ci} and v_{ci} where $u_{ci} = u(p_i)$ and $v_{ci} = v(p_i)$.

As stated before, the coordinate frame of the measurement system and the coordinate frame of the CAD model rarely coincide. The deviation of the point set frame from the model frame can be quantified by the sum of the d_i squared as shown in Eq. (2). The d_i values are squared to eliminate vector direction issues and to target the vector magnitude.

$$f = \sum_{i=1}^n \|d_i\|^2 = \sum_{i=1}^n (d_i^T \cdot d_i) \quad (2)$$

The points in P are rigid bodies in three-dimensional space and, therefore, can move in six degrees of freedom. The six degrees consist of three orthogonal translations and three orthogonal rotations. The translations can be formulated into a \mathcal{R}^3 vector to be added to the points in P , and the rotations formulated into a $\mathcal{R}^{3 \times 3}$ orthogonal matrix. Defining the translation vector as t and the rotation matrix as R , Eq. (3) reveals the means of transforming P into a new coordinate frame.

$$p'_i = R p_i + t \quad (3)$$

The translation vector, t , is simple to understand, but the rotation matrix is more complex. Various ways of representing the parameters that specify this matrix have been used in the solution of the registration problem. One of the more simple approaches is the use of the angles of rotation about the three principal axes of a

fixed coordinate system. Using this approach, R is a function of θ_x , θ_y , and θ_z , where θ_i represents the angle of rotation about the i th axis. Considering t to consist of t_x , t_y , and t_z , the six degrees of freedom can be collected in to the following \mathfrak{R}^6 vector of parameters:

$$X = [\theta_x \ \theta_y \ \theta_z \ t_x \ t_y \ t_z] \quad (4)$$

Now, Eq. (3) reassembles into a function of X given by

$$p'_i = p_i(X) = R(X)p_i + t(X) \quad (5)$$

Substituting Eq. (5) into Eq. (1) yields

$$d_i(X) = p(X) - S(u_{ci}(X), v_{ci}(X)) \quad (6)$$

In Eq. (6), the minimization is now represented by the substitution of u_{ci} and v_{ci} into u and v in Eq. (1). Also, u_{ci} and v_{ci} are now shown as functions of X since u_{ci} and v_{ci} are functions of p , and p is a function of X . Substituting Eq. (6) into Eq. (2) maps f into a function of X as shown below in Eq. (7).

$$f(X) = \sum_{i=1}^n (\|d_i(X)\|^2) \quad (7)$$

In order to transform the coordinate frame of the point set such that it coincides with the coordinate frame of the model as much as possible, the function f must be minimized with respect to the six rigid body transformation parameters specified in X . The X that provides this minimum is the solution to the registration problem.

The function f is nonlinear and requires iterative minimization routines to solve for the optimal X value. Iterative minimization typically involves successively changing the value of X by a calculated step vector until the minimum is achieved. The procedure must converge or move closer to the solution after every iteration. The iterations cease when the convergence criteria have been met.

From multivariate calculus, for X^* to be a local minimum, it is necessary that

$$\nabla f(X^*) = 0 \quad (8)$$

and

$$\nabla^2 f(X^*) \text{ is positive semidefinite} \quad (9)$$

The most common convergence criterion is that the gradient of f , represented by Eq. (8), is close to zero within a given tolerance. The function f may be twice differentiable in X , but the gradient as well as Hessian as given by Eqs. (8) and (9), respectively, may not be easily obtained due to the nonlinearities involved. If this information can be calculated, both can then be used in the iterative minimization to determine step size and direction.

The Hessian provides information on whether a minimum or a maximum of the function occurs at the stationary point defined by Eq. (8). However, the iterative nature of optimization routines already provides this information since one can observe whether a function is increasing or decreasing from one iteration to the next. The second-order information is useful for determining step sizes and directions, but not required for determining whether the goal has been obtained. The calculation of first-order information is valuable not only for step calculation but also for convergence determination. Methods that do not use gradient information or an approximation thereof are heuristic and cannot be as exact as gradient-based methods. In inspection applications where levels of certainty and precision must be maintained, gradient-based methods are essential. Finite difference gradients can be employed, but are computationally expensive in terms of time. Analytical gradients, if available, provide faster minimization without large computational expense.

Analytical gradients for simple shapes can be calculated in a straightforward manner. Typically, analytic expressions for the point to surface distance, d_i , are available for simple shapes (e.g., planes and quadric objects such as spheres and cylinders). For

higher-order polynomials such as Bezier or b -spline surfaces, the problem is more complex. Consider a parametric spline surface, S , of order m . In order to determine the parameters corresponding to the closest point on S , the following nonlinear system of equations must be solved.

$$\frac{\partial d_i}{\partial u} = \frac{1}{2} \frac{1}{\|p_i - S(u, v)\|} \left[(p_i - S(u, v))^T \cdot \frac{\partial S(u, v)}{\partial u} \right] = 0 \quad (10)$$

$$\frac{\partial d_i}{\partial v} = \frac{1}{2} \frac{1}{\|p_i - S(u, v)\|} \left[(p_i - S(u, v))^T \cdot \frac{\partial S(u, v)}{\partial v} \right] = 0 \quad (11)$$

This system can be reduced to

$$(p_i - S(u, v))^T \cdot \frac{\partial S(u, v)}{\partial u} = 0 \quad (12)$$

$$(p_i - S(u, v))^T \cdot \frac{\partial S(u, v)}{\partial v} = 0 \quad (13)$$

Equations (12) and (13) above represent two $2m - 1$ degree polynomials in both u and v . As this system is extremely nonlinear, it must be solved numerically. Typically, Newton methods [19] are employed to solve for u and v . Such procedures are often referred to as point projection, and many texts provide detailed algorithms addressing this problem [20]. Point projection must be performed for all points in the set P to determine u_{ci} and v_{ci} .

Now, consider the problem of finding the gradient of f . By taking the derivative of f with respect to an arbitrary member of X defined as ξ one can gain insight into the registration of S to P .

$$\frac{\partial f}{\partial \xi} = 2 \sum_{i=1}^n \left(d_i \cdot \frac{\partial d_i}{\partial \xi} \right) \quad (14)$$

Given that d_i can be found by the procedures discussed in the last paragraph, let us concentrate on the \mathfrak{R}^3 vector derivative of d_i . Equation (15) shows d_i as a function of ξ .

$$d_i(\xi) = p_i(\xi) - S(u_{ci}(\xi), v_{ci}(\xi)) \quad (15)$$

The partial of d_i is then

$$\frac{\partial d_i(\xi)}{\partial \xi} = \frac{\partial p_i(\xi)}{\partial \xi} - \frac{\partial S(u_{ci}(\xi), v_{ci}(\xi))}{\partial \xi} \quad (16)$$

The partial of p_i can be calculated as shown in previous research [21], but the partial of S has yet to be discovered. Using multivariate chain rule [22], the partial of S can be broken down into

$$\frac{\partial S(u_{ci}(\xi), v_{ci}(\xi))}{\partial \xi} = \frac{\partial S(u_{ci}, v_{ci})}{\partial u} \frac{\partial u_{ci}}{\partial \xi} + \frac{\partial S(u_{ci}, v_{ci})}{\partial v} \frac{\partial v_{ci}}{\partial \xi} \quad (17)$$

The partials of S with respect to u and v can be determined from standard routines [19]. The problem is now reduced to finding the partials of u and v with respect to ξ . The parameters u and v are given by the system of equations in Eqs. (10) and (11). This system is rewritten here to show the dependence on ξ .

$$(p_i(\xi) - S(u_{ci}(\xi), v_{ci}(\xi)))^T \cdot \frac{\partial S(u_{ci}(\xi), v_{ci}(\xi))}{\partial u} = 0 \quad (18)$$

$$(p_i(\xi) - S(u_{ci}(\xi), v_{ci}(\xi)))^T \cdot \frac{\partial S(u_{ci}(\xi), v_{ci}(\xi))}{\partial v} = 0 \quad (19)$$

While the partials cannot be supplied by solving the system above for differentiable expression of u and v , a large amount of information is available after a point projection has been performed for p_i at a given value of ξ . In his research, Tucker [23] has developed the partials of u and v with respect to the rigid body parameters based on information available once point projection has been performed. Using these results, analytic gradient information is used in the minimization of the sum of the squares [23–25].

Table 2 Gear nomenclature

A	Inner hub
B	Outer hub
C	Web ring
D	Addendum circle
E	Keyway flat
F	Web arm
G	Gear profile

Results

The alignment of the 670,000 points to the target CAD model was completed using algorithms based on complete gradient information using an enhanced Gauss Newton approach. The target CAD model was comprised of all analytic surfaces consisting of 1814 planes and 32 cylinders (see Fig. 4(d)). The nomenclature used for the CAD model is presented in Fig. 4(d) and Table 2. Registration time was approximately 2 min on a PC using a 2-GHz Pentium IV processor with 500 Mbytes of RAM. Figure 4(e) shows a colored error map for normal point-to-surface deviations between the CAD model and the 3D data. Resolution of the original images is much greater than can be seen in the versions printed here.

Calculations were also performed to measure the dimensions of certain key geometries in the gear such as the hub radius, tooth thickness, addendum circle and various sidewall angle deviations. The results of these analyses are presented in Table 3. Because no addendum circle datum was available in the CAD model, this dimension was measured using measuring point-to-point distances. Ten diameters were measured on three separate cross sections throughout the extrusion height of the gear to compute the addendum circle radius. It should be noted that large deviations in gear thickness are expected due to the LIGA release and lapping process. For this gear, the sidewalls should be perpendicular to the base and top of the gear. Table 4 presents the mean sidewall deviation for the various features. To generate the values in Table 4, sidewall deviation values for each individual surface were determined and subsequently averaged.

3D Metrology Using Digital Volumetric Imaging. Using DVI techniques for data collection and Paraform (www.paraform.com) software for analysis and inspection, a 664- μm (nominal), 62-tooth nickel gear was imaged and measured. Both absolute dimensions and sidewall angles were examined. Additional software capabilities could enable the examination of gear tooth involutes, pitch, and other critical data. Values for the absolute dimensions and the sidewall angles can be found in Tables 3 and 4. For most of the gear geometries, there were several surfaces with the same nominal dimensions. For example, there are two half cylinders that comprise the inner hub, both of

Table 3 Absolute dimensions for gear geometry.* Because no addendum circle datum was available in the CAD model, this dimension had to be taken by hand by measuring point-to-point distances. Ten diameters were measured on three separate cross sections throughout the extrusion height of the gear. Paraform software provided the distance calculation.

Feature	Nominal dimension (μm)	As-built dimension (μm)	Deviation (μm)
Inner hub radius	100	101	+ 1
Outer hub radius	150	151	+ 1
Web circle radius	275	275	0
Addendum circle radius	264	659*	- 5
Gear thickness	150	161*	+ 11

*As mentioned before, such large deviations in gear thickness were somewhat expected due to the LIGA release and lapping process.

Table 4 Sidewall angles for LIGA gear

Feature	Angular Deviation (degrees)
Inner hub	0.4
Outer hub	0.3
Web circle	0.2
Web arms	0.3
Keyway flats	0.1

which should have a radius of 150 μm . In making such measurements, the mean values between all related geometries were calculated and presented.

In addition to providing statistical information about certain absolute dimensions in the dataset, the inspection module in Paraform allowed for visual inspection of surfaces through error mapping (Fig. 5, Fig. 6(b,c)). As can be seen in Fig. 5, the gear varies from the CAD model in unpredictable ways. This particular gear varies about $\pm 5 \mu\text{m}$ from various nominal surfaces, mainly the top and bottom profiles of the gear. One would expect such large deviations along the axis of the gear due to the process in which the plated gears are lapped and removed from the PMMA molds. Dark areas at the tips of the gear are places where data are missing.

As good as the images created by DVI are [7] as discussed in the experimental section, some challenges need to be overcome for cutting hard materials. For example, the diamond microtome blades used to slice off the thin sheets of metal/embedding polymer are almost “atomically sharp” at the beginning of the cutting sequence. (We were unable to resolve an edge on the blade using an Hitachi 2700 SEM.) The hardness (values ranging from 500 to 700 HV) and high strength (σ_y values ranging from 1.0 to 1.4 GPa) of the metal, as compared to tissue and polymer samples, chips and degrades the knife edge, causing striations in the cut face. These striations can introduce noise at the surface boundaries of the part, producing artifacts at that location in the segmented surface. A single blade was used for all cuts on a given sample, and was typically sent for resharpening after a each sample. Blades last for numerous cuts on soft materials, and blade damage does not typically show up when cutting soft materials. Experiments are currently underway to determine a better cutting material (boron nitride or various carbides) or a better angle to use at the cutting edge. One of the authors of Ref. [15] has stated to us that the choice of diamond knife brand is more critical than we had anticipated [26]; thus we will also test different knife brands for effectiveness in cutting. We also plan to develop a surface lubrication technique. Hard LIGA plating materials such as nickel alloys often resist cutting so strongly that parts are ejected from the embedding polymer before they can be fully imaged. Use of the adhesion promoter (below) alleviates this problem.

The tables presented represent the mean sidewall deviation for the various features. Paraform software provides information about the sidewall deviation for each individual surface, and these values were then averaged for presentation purposes.

System Calibration

Resolution Sciences currently calibrates its microscopes with a NIST-traceable line scale, which provides accountability for measurements in the x and y directions. There is currently no way to characterize the entire 3D precision of the system, due to the unavailability of a traceable 3D standard. We decided to use ball bearings as calibration standards. Precision steel balls cannot be easily cut using DVI do to their extreme hardness, although ball bearings possibly represent the ideal 3D calibration standard due to the extreme precision with which they can be made [27]. Work continues to learn how to cut high-precision steel balls as the ideal calibration of the system.

To calibrate the system, we imaged several inexpensive one-sixteenth in. (1.588 micron) ($\Phi \frac{1}{16} \pm 0.001$ in.) brass ball bearings

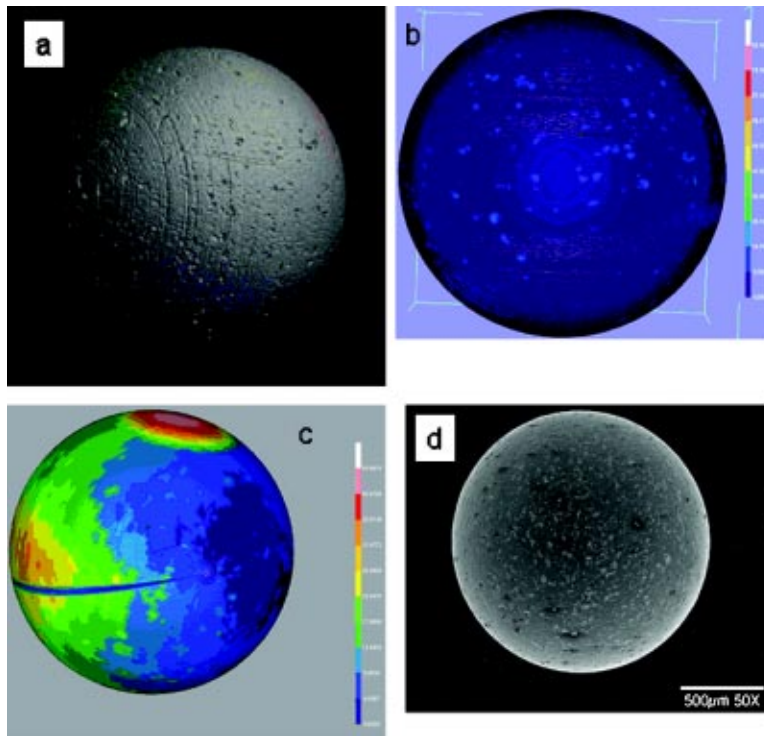


Fig. 6 (a) A DVI image of a brass ball bearing. (b) That same ball imaged relative to a sphere model, showing surface defects. (c) A DVI image of another ball matched to a CAD model of a sphere, which shows imperfections in the manufacturing process. The region at the top is missing data where the remaining partial sphere fell out of the mold. (d) A SEM image of a brass ball for comparison. DVI shows surface phenomena that cannot be seen by SEM. The original DVI images are in color. These ball bearings have been measured by a variety of techniques. Using calipers, the ball measured 1.54–1.57 mm, using a calibrated SEM image by counting pixels, the ball measured 1.567 mm, with an edge selected by eyeball, and using DVI we measured 1.571 and 1.568 mm in *X* and *Y* directions. The errors noted are typical—as can be seen from the images above, the exact location of the surface varies.

from McMaster Carr. Holding any spherical object is difficult—initially balls popped out of the mold after cutting about half of the ball away. To alleviate this problem, balls were treated with an adhesion promoter, Dow Z-6030 (trimethoxysilylpropyl methacrylate), about a 2% solution in alcohol. This allowed us to cut some balls completely. As can be seen by the images, Fig. 6, surface detail shows up when the DVI image is matched to the CAD model that is unavailable in any other way. The spiral pattern is due to the way ball bearings are made, by rolling in between two plates. This particular ball did not roll on all three axes, rather it wobbled or precessed around between the plates, not getting ground on the ends. Then it flipped axes of rotation and a few streaks were ground around one side. These are low-quality balls—high-quality balls [27] have much better surface finishes.

To demonstrate that interior defects can be seen using DVI, Fig. 7 show a microspring made by plating of a very hard nickel alloy. Figure 7(a) shows the exterior of the entire spring, with some visible surface defects. To show that the defects are more than cosmetic, Fig. 7(b) shows a sectioning of the same spring, demonstrating that some the defects are larger in the body of the spring than on the surface, and that some defects are only on the surface. Figure 8 shows how fine the detail of the oval hole in two dimensions.

Conclusion and Summary

DVI is a new and unique way to image 3D micromachines. By exporting the DVI image into a modeling program, the original

device can be compared to the CAD model, showing surface and interior detail unobtainable using any other method. This allows for accurate metrology of complex structures. We have developed methods to calibrate the system in three dimensions using ball

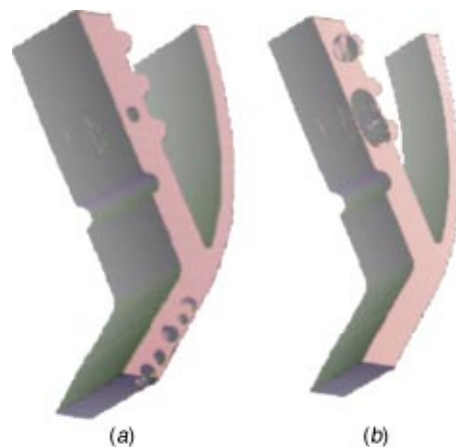


Fig. 7 (a) A complete nickel alloy spring with surface defects. (b) A deeper section of the same part, showing that the bottom defects are primarily on the surface, but the one small hole near the top leads to a large void within the spring.



Fig. 8 A 2D image of the oval void in Fig. 6 showing the fine detail of this imaging technique.

bearings and silver wire embedded at a precise angle with respect to the optical axis.

Improved knife materials and methods need to be developed to cut hard metals, and use of a surfactant has allowed the polymer embedding matrix to adhere to the metal well enough to image complete spheres. The use of a lubricant will improve cut face surfaces, and the use of an etchant to allow 3D visualization of metal grain boundaries is being explored.

This paper presents the algorithms used for exact metrology of three-dimensional coordinate data from a microcomponent. In particular, a Digital Volumetric Imaging machine produced a 3D image of the microcomponent that was then used to generate a point cloud of data. This point cloud was compared to its nominal or target geometry via a least-squares fit using a modified Gauss-Newton approach for registration. The resulting registration enabled an overall geometric comparison via a point-to-surface deviation calculation. The overall deviation of the gear was at most $11\ \mu\text{m}$ from nominal. Most of this deviation was from the LIGA release and lapping process. Other dimensions that are not directly affected by the release and lapping processes were controlled to tighter specifications (e.g., less than $5\ \mu\text{m}$).

Acknowledgment

Sandia National Laboratories is multiprogram laboratory operated by Sandia Corporation, a Lockheed Martin Company for the U.S. Department of Energy's National Nuclear Security Administration under Contract No. DE-AC04-94AL85000.

References

- [1] Soleyky, E., Archie, C., Hayes, T., Banke, B., and Cornell, R., 2001, "Three Dimensional Top Down Metrology: A Viable Alternative to AFM or Cross Section?," *Metrology, Inspection and Process Control for Microlithography XV*, N. T. Sullivan, ed., Proc. SPIE, **4344**, p. 366–376.
- [2] Russ, J. C., 2002, *The Image Processing Handbook*, 4th ed., CRC Press, Boca Raton, FL.
- [3] Udupa, J. K., and Herman, G. T., eds., 2000, *3D Imaging in Medicine*, 2nd ed., CRC Press, Boca Raton, FL.
- [4] Osten, W., Seebacher, S., and Jeptner, W., 2001, "The Application of Digital Holography for the Inspection of Microcomponents," Proc. SPIE, **4400**, pp. 1–15. Other papers in this volume also discuss 3D imaging and measurement.
- [5] Franco, E., Chang, W., and Morales, A., 2002, "Non-Destructive Creation of Accurate 3D Images of MEMS Microcomponents," unpublished results.
- [6] Pourciel, J. B., Jalabert, L., and Masuzawa, T., 2002, "SDAPPLIN, A Method for 2-D Profiling on High Aspect Ratio Microstructures. Improvement for 3D Surfacing," Mitsubishi, M., Kurfess, T., ed., *Proc. 2002 Japan-USA Symposium on Flexible Automation, Hiroshima, Japan, July, 2002*, p. 553–555. Published by the Institute of Systems, Control and Information, Kyoto, Japan.
- [7] Sinha, G., 2001, *Popular Science*, Dec., pp. 80–83.
- [8] Ewald, A. J., McBride, H., Reddington, M., Fraser, S. E., and Kerschmann, R., 2002, "Surface Imaging Microscopy, an Automated Method for Visualizing Whole Embryo Samples in Three Dimensions at High Resolution," *Top. Mol. Organ. Eng.*, **225**, pp. 369–375.
- [9] Madou, M., 1997, *Fundamentals of Microfabrication*, CRC Press, Boca Raton, FL.
- [10] The Sandia LIGA website, <http://www.ca.sandia.gov/liga/>
- [11] U.S. Patent No. 4,960,330, Image Recording Device, Russell L. Kerschmann.
- [12] The website containing Digital Volumetric Imaging information, www.micro-sciencegroup.com
- [13] Swab, P., 1995, "Ultramicrotomy of Diamond Films for TEM Cross-Section Analysis," *Microsc. Res. Tech.*, **31**, pp. 308–310.
- [14] Barreto, M. P., Veillette, R., and L'Esperance, G., 1995, "Development and Application of a Dry Ultramicrotomy Technique for the Preparation of Galvanneal Sheet Coatings," *Microsc. Res. Tech.*, **31**, pp. 293–299.
- [15] McMahon, G., and Malis, T., 1995, "Ultramicrotomy of Hard Materials," *Microsc. Res. Tech.*, **31**, pp. 267–274.
- [16] Glanvill, S. R., 1995, "Ultramicrotomy of Semiconductors and Related Materials," *Microsc. Res. Tech.*, **31**, pp. 275–284.
- [17] Claudet, A., 2001, "Analysis of Three Dimensional Measurement Data and Multi-Surface CAD Models," Ph.D. dissertation, School of Mechanical Engineering, Georgia Institute of Technology, Atlanta, GA.
- [18] Claudet, A., and Kurfess, T., 2002, "Analysis of 3D Measurement Data for Micro-Systems," Mitsubishi, M., Kurfess, T., eds., *Proc. of the Japan-USA Symposium on Flexible Automation, Hiroshima, Japan, July, 2002*, pp. 250–252. Published by the Institute of Systems, Control and Information, Kyoto, Japan.
- [19] Dennis, J. E., Jr., and Schnabel, R. B., 1996, *Numerical Methods for Unconstrained Optimization and Nonlinear Equations*, SIAM, Philadelphia.
- [20] Peigl, L., and Wayne T., 1997, *The NURBS Book: Monographs in Visual Communication*, 2nd ed., Springer, New York.
- [21] Claudet, A., 1998, Master thesis, "Data Reduction For High Speed Computational Analysis of Three Dimensional Coordinate Measurement Data," Master's thesis, School of Mechanical Engineering, Georgia Institute of Technology, Atlanta, GA.
- [22] Shenk, A., 1998, *Calculus and Analytic Geometry*, 4th ed., Scott, Foresman and Company, Boston.
- [23] Tucker, T. M., 2000, "A New Method for Parametric Surface Registration," Ph.D. dissertation, School of Mechanical Engineering, Georgia Institute of Technology, Atlanta, GA.
- [24] Tucker, T. M., and Kurfess, T. R., 2003, "Newton Methods for Parametric Surface Registration: Part I: Theory," *Comput.-Aided Des.*, **35**, pp. 107–113.
- [25] Tucker, T. M., and Kurfess, T. R., 2003, "Newton Methods for Parametric Surface Registration: Part II: Experimental Validation," *Comput.-Aided Des.*, **35**, pp. 114–120.
- [26] T. Malis, 2003, personal communication.
- [27] Private communication and unpublished paper by Eugene Gleason, 2002, Bal-tec Corporation, Los Angeles, CA. Bal-tec and other bearing manufacturers have developed sophisticated and precise ways to measure ball bearings.